Supplementary Material
Developing a novel continuum model of static and dynamic contact angles: A case study of a water droplet on micro-patterned hybrid substrates

Arash Azimi, Chae Rohrs, Ping He*, Chun-Wei Yao
Department of Mechanical Engineering, Lamar University, Beaumont, TX 77710

1. Convergence study

To determine the spatial and temporal convergence, a series of simulations have been performed for (1) different grid sizes ($\Delta x = 50$, 25, 20 and 12.5 μm) at the same time step, $\Delta t =$ 0.002 ms, and (2) different time steps ($\Delta t = 0.001$, 0.002, 0.004 and 0.008 ms) at the same grid size, $\Delta x = 50\ \mu m$. In each individual case, the relative errors are evaluated using Eqs. (S1-S2).

$$L_{1,norm} = \frac{\sum_{n=1}^{N} |f_n - f_{exact,n}|}{N} \tag{S1}$$

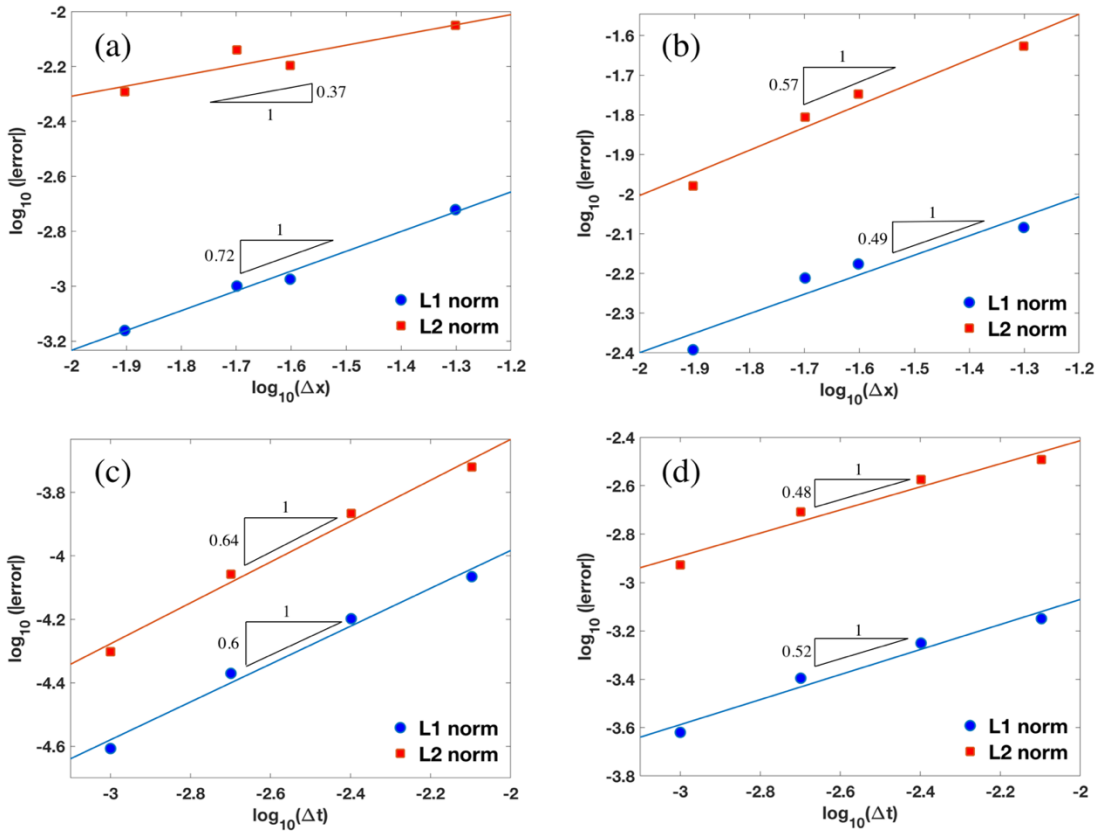

Figure S1. The spatial convergence rate at $\Delta t = 0.002$ ms: (a) The convergence rate for pressure, and (b) velocity; the temporal convergence rate at Δx =50 μm: (c) The convergence rate for pressure, and (d) velocity. The slopes represent the convergence rates.

* Corresponding author. Email: phe@lamar.edu. Tel: (409) 880-7129.

$$L_{2,norm} = \left[\frac{\sum_{n=1}^{N}\left|f_n - f_{exact,n}\right|^2}{N}\right]^{1/2} \quad \text{(S2)}$$

where N is the total selected cell numbers, f_n is the value of the numerical solution at cell n, and $f_{exact,n}$ is the exact solution, which is extrapolated from the numerical solutions. $L_{1,norm}$ and $L_{2,norm}$ represent the lowest convergence rate and the average convergence rate, respectively. Fig. S1 shows the spatial and temporal convergence rates.

2. Equilibrium contact angle measurements

All of the apparent contact angles in our simulations are measured using the KRUSS ADVANCE software. Fig. S2 shows the equilibrium contact angles at different substrates.

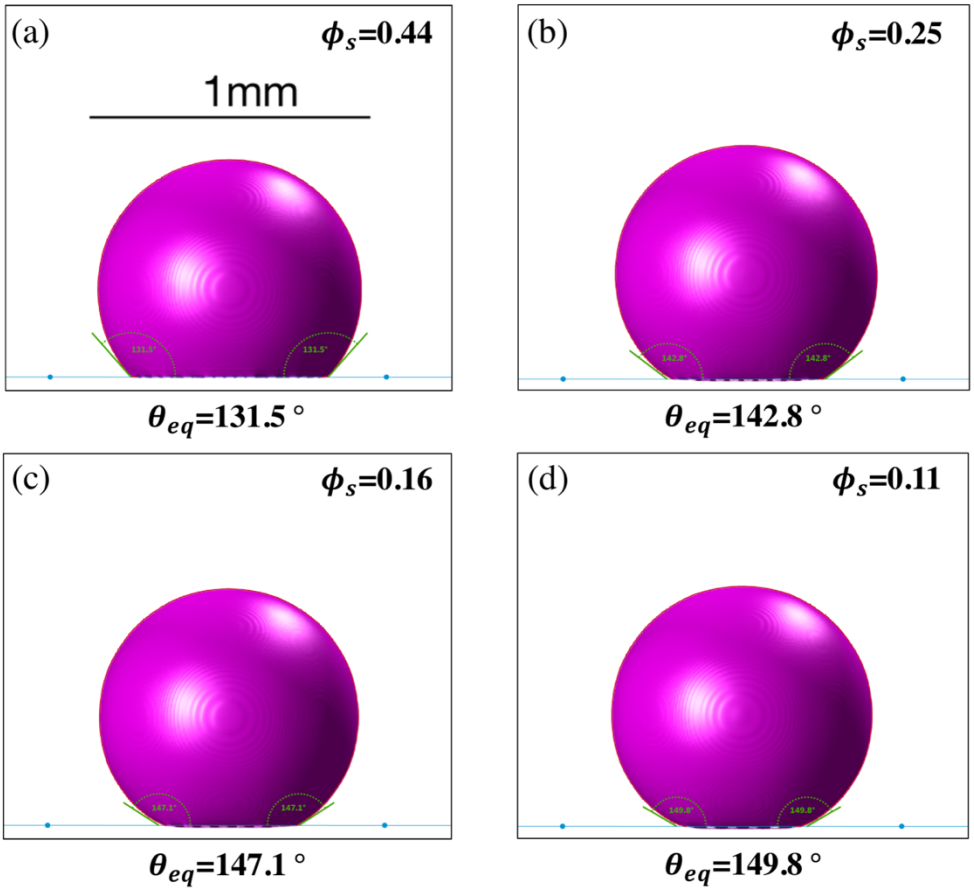

Figure S2. Apparent contact angle at equilibrium measured using KRUSS ADVANCE for (a) $\phi_s = 0.44$, (b) $\phi_s = 0.25$, (c) $\phi_s = 0.16$, and (d) $\phi_s = 0.11$.

3. Dynamic receding movies

Fig. S3-S6 show the snapshots of the receding movies at different substrates and views.

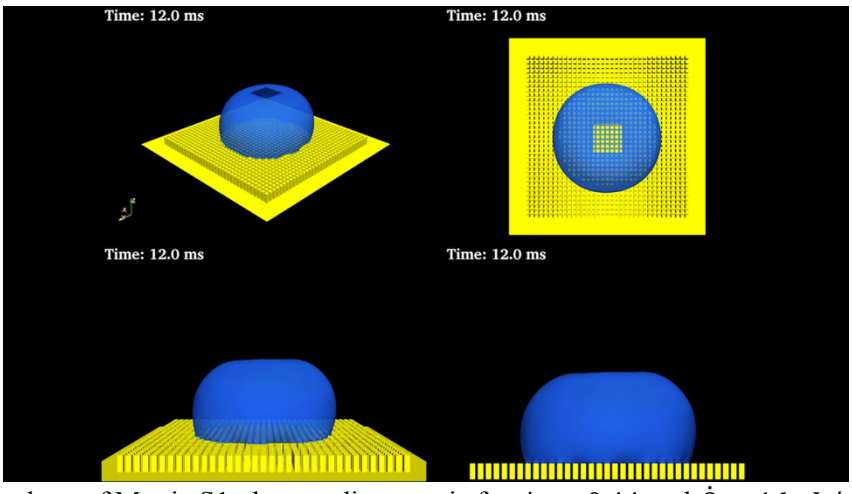

Figure S3. Snapshots of Movie S1, the receding movie for $\phi_s = 0.44$ and $\dot{Q} = 16$ μL$/s$: 3D view, top view, 3-D side view, and 2-D side view.

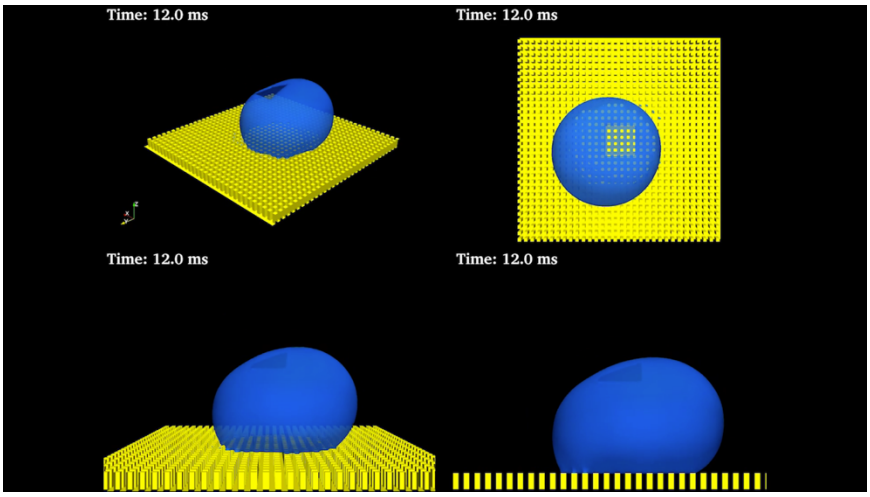

Figure S4. Snapshots of Movie S2, the receding movie for $\phi_s = 0.25$ and $\dot{Q} = 16$ μL$/s$.

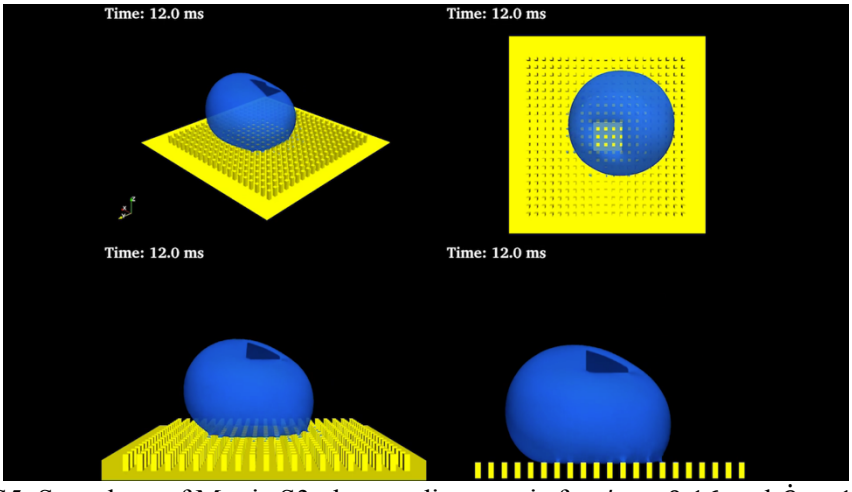

Figure S5. Snapshots of Movie S3, the receding movie for $\phi_s = 0.16$ and $\dot{Q} = 16$ µL/s.

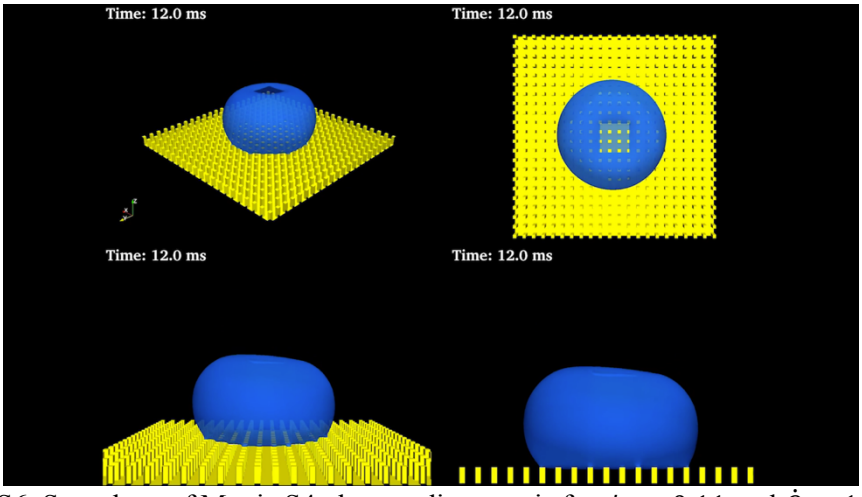

Figure S6. Snapshots of Movie S4, the receding movie for $\phi_s = 0.11$ and $\dot{Q} = 16$ µL/s.

4. Dynamic advancing movies

Fig. S7-S10 show the snapshots of the advancing movies.

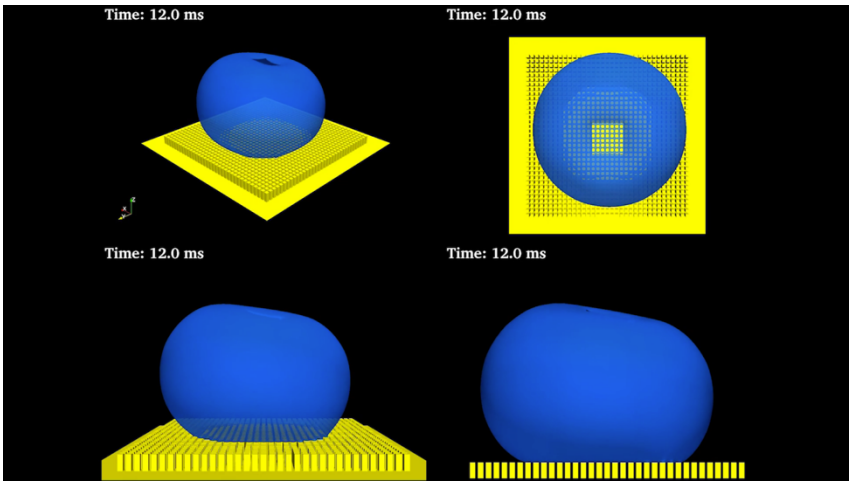

Figure S7. Snapshots of Movie S5, the advancing movie for $\phi_s = 0.44$ and $\dot{Q} = 16$ μL/s.

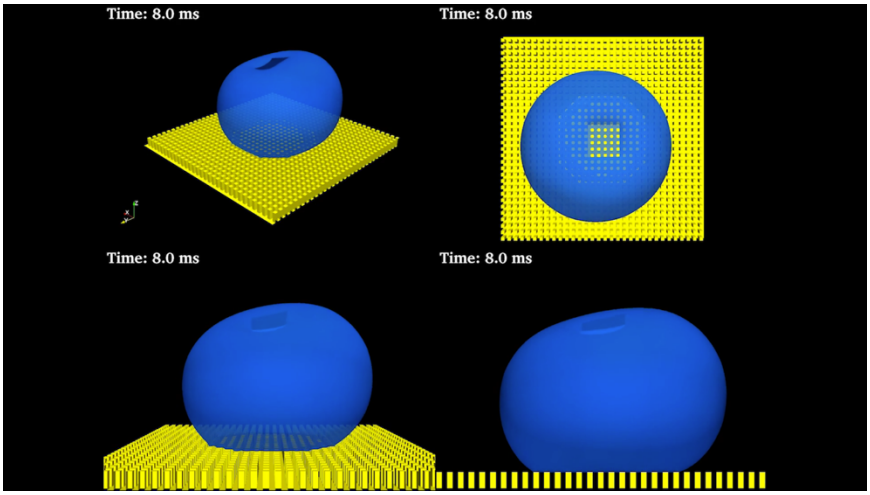

Figure S8. Snapshots of Movie S6, the advancing movie for $\phi_s = 0.25$ and $\dot{Q} = 16$ μL/s.

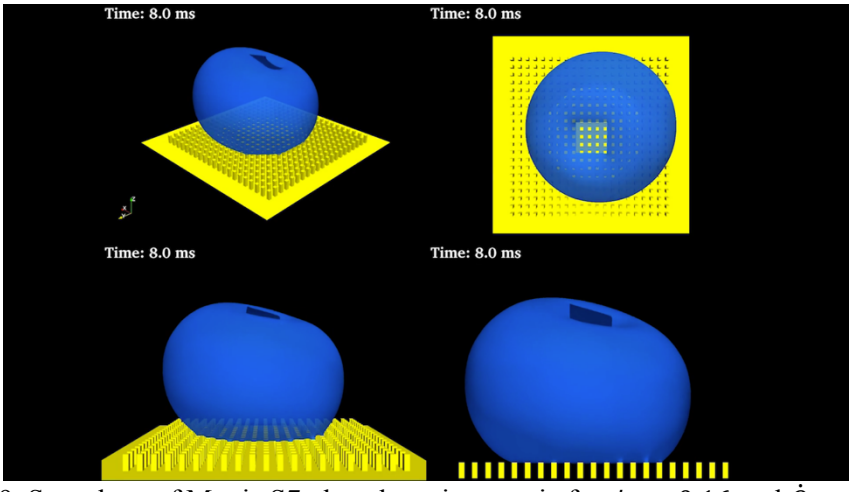

Figure S9. Snapshots of Movie S7, the advancing movie for $\phi_s = 0.16$ and $\dot{Q} = 16\ \mu L/s$.

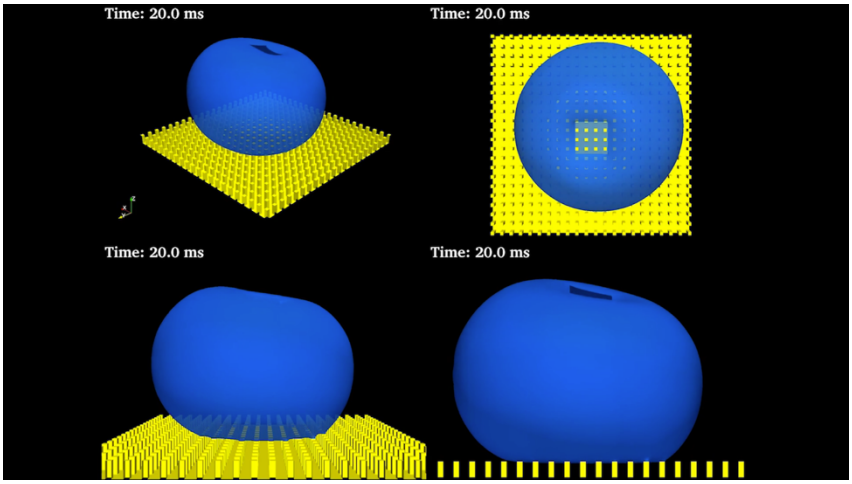

Figure S10. Snapshots of Movie S8, the advancing movie for $\phi_s = 0.11$ and $\dot{Q} = 16\ \mu L/s$.

5. Penetration and sagging

Fig. S11-S12 depict the penetration and sagging of the droplet at different ϕ_s for the equilibrium and advancing modes, respectively.

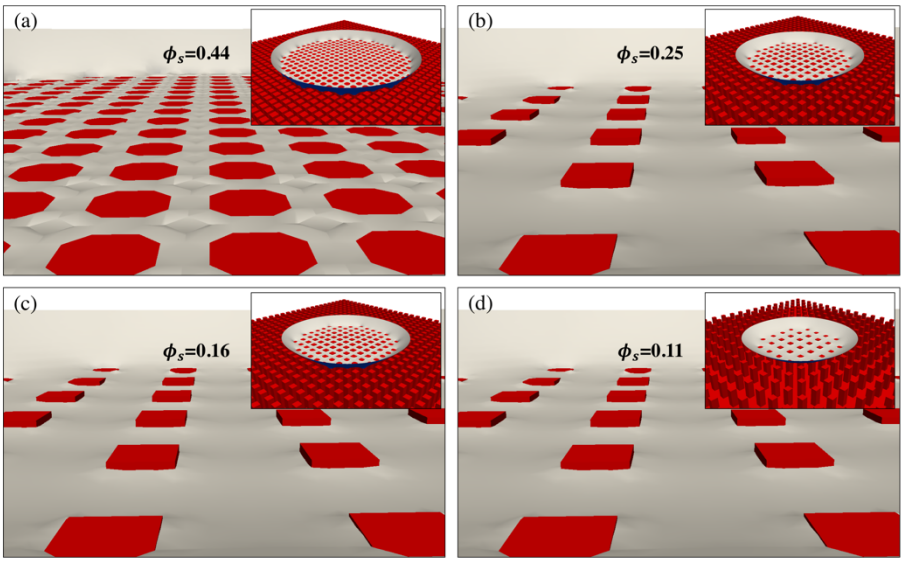

Figure S11. The penetration and sagging at the equilibrium state. Micro-patterned substrate is in red, water droplet in light gray, and a cut view of the water droplet bottom surface is shown in a small window on the top-right corner: (a) $\phi_s = 0.44$, (b) $\phi_s = 0.25$, (c) $\phi_s = 0.16$, and (d) $\phi_s = 0.11$.

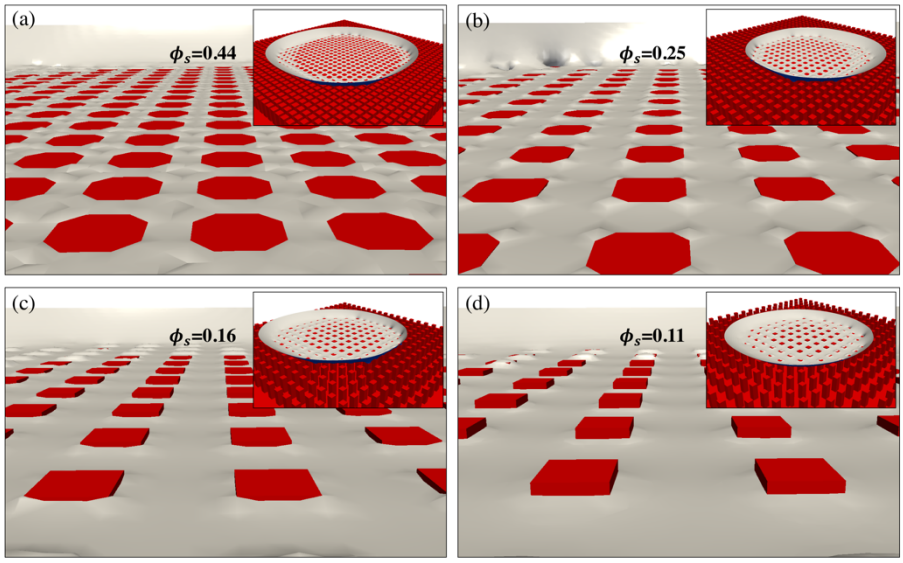

Figure S12. The penetration and sagging at the advancing mode: (a) $\phi_s = 0.44$, (b) $\phi_s = 0.25$, (c) $\phi_s = 0.16$, and (d) $\phi_s = 0.11$.

6. Effect of liquid viscosity near solid

The effect of liquid viscosities near the solid surface, μ_s, have been illustrated in Fig. S13. The difference of the equilibrium contact angle is just 0.2° between $\mu_s = 10$ cP and $\mu_s = 100$ cP as shown in Fig. S13a and b. Fig. S13c and d show the evolution of the center of droplet in *z*-direction and liquid-solid contact area, respectively. The relative differences in Fig. S13c and d normalized by the droplet diameter and total surface area, respectively, are both around 0.2%.

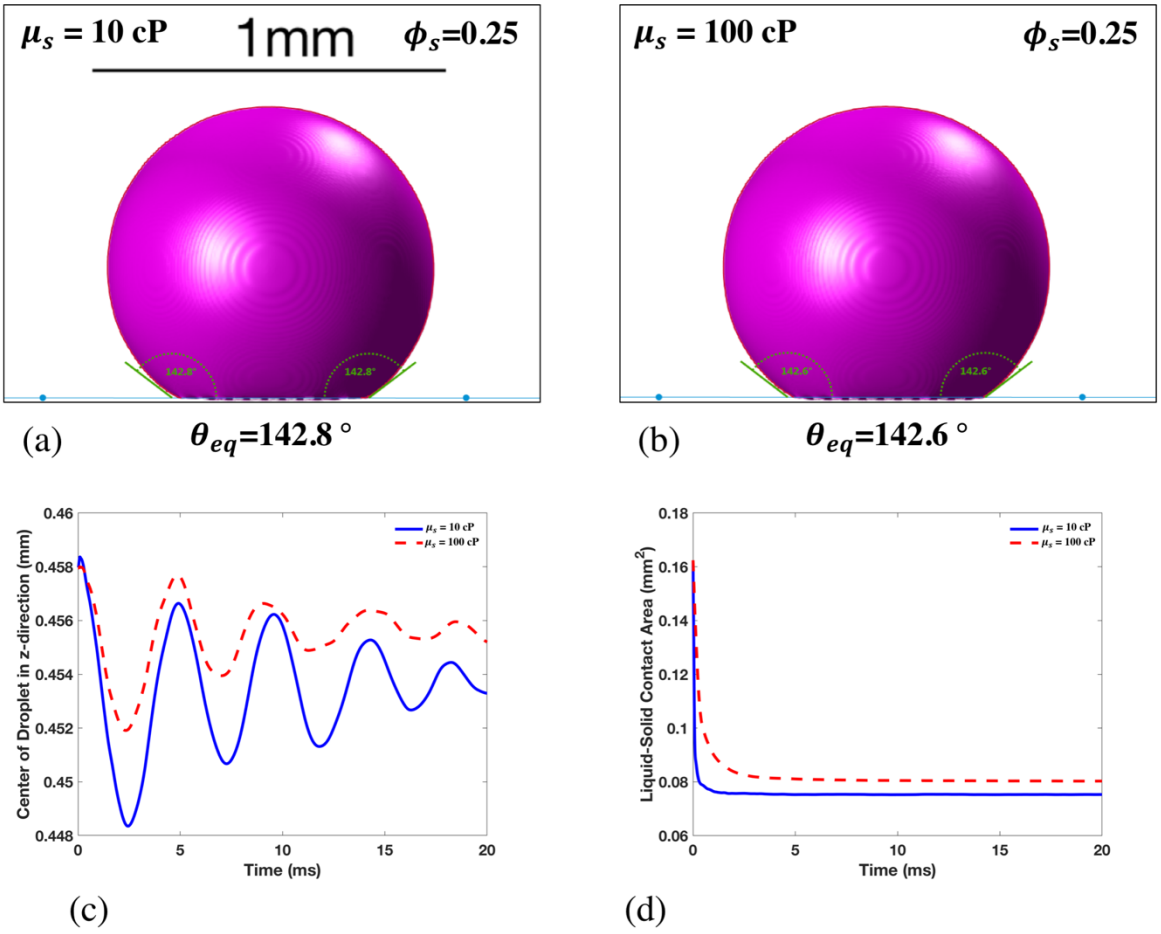

Figure S13. Effect of liquid viscosity near solid: Droplet contour and measured equilibrium contact angle at (a) $\mu_s = 10$ cP, and (b) $\mu_s = 100$ cP; (c) evolution of the droplets center, and (d) liquid-solid contact area at different μ_s.

7. Simulation physical parameters

The following physical parameters are used in all simulations in this paper: water density ρ_L=1000 kg/m^3, water viscosity μ_L=1 cP, air density ρ_G=1 kg/m^3, air viscosity μ_G=14.8 μPa·s, and water-air surface tension σ=70.7 mN/m.